Retrieval Hyperspectrally-Resolved Surface IR Emissivity

Daniel K. Zhou, Allen M. Larar, Xu Liu, William L. Smith,
L. Larrabee Strow, P. Yang, and Peter Schlüsse

OUTLINE:

- Motivation & Goal
- Ret. Algorithms & Cloud Detection
- Retrieval Analysis and Demo.
- Evaluation with Lab. Samples
- Quality Filter for Monthly Mean
- Seasonal Variation
- Summary and Future Work

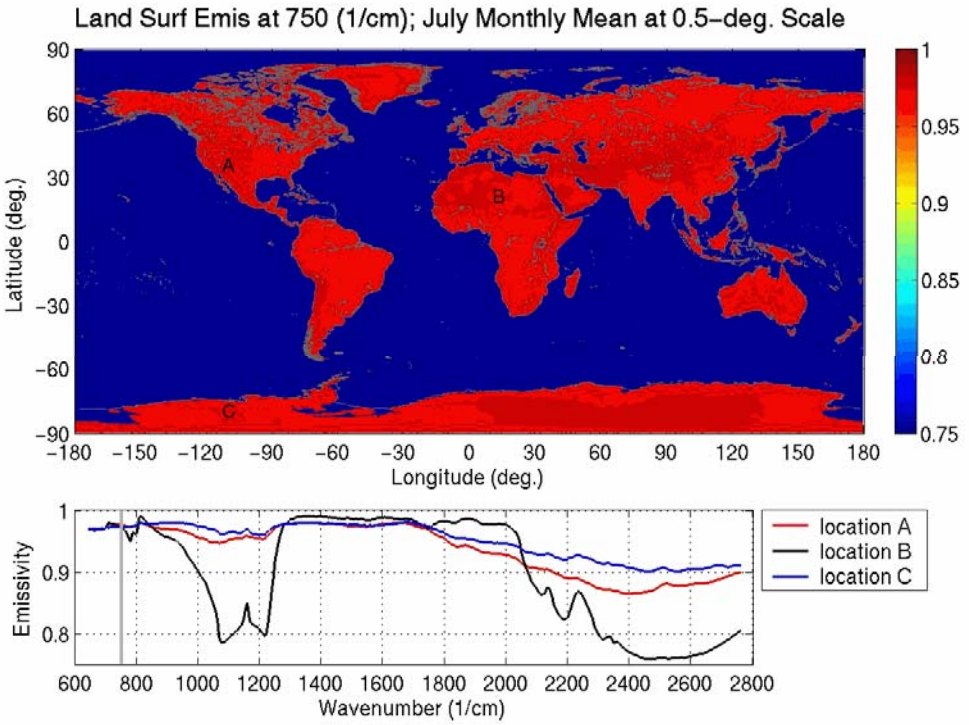

Motivation & Goal

Study Earth from space to improve our scientific understanding of global climate change; derive global IR spectral emissivity with hyperspectral IR measurements from operational satellites.

1.IR hyperspectral radiance measurements are available from current AIRS (since May 2002) and IASI (October 2006), and will be available from future operational weather satellites.

2.Land surface emissivity and skin temperature from the current and future operational satellites can, and will, reveal critical information on the Earth's land surface type properties and Earth's ecosystem.

3.Long-term and large-scale observations, needed for global change monitoring and other research, can only be supplied by satellite remote sensing.

4.Accurate surface emissivity retrieved from satellite measurements are beneficial to

- helping to understand the nature of radiative transfer process for the Earth and atmospheric environment,
- assisting assimilation of hyperspectral IR radiances in NWP models,
- improving retrieval accuracy for other thermodynamic parameters (e.g., T_s, CO, CO_2, O_3, H_2O),
- helping surface skin temperature retrieval from other satellite broad-band measurements,
- improving accuracy of surface radiation budget calculation for climate studies, and
- long-term monitoring of the global environment and climate change.

Hyperspectral Emis. Ret. Algorithms

C. C. Borel (1998): Surface emissivity and temperature retrieval for a hyperspectral sensor, *Geoscience and Remote Sensing Symposium Proceedings*, **1**, 546-549.

*__D. K. Zhou et al. (2002):__ Thermodynamic product retrieval methodology for NAST-I and validation, *Appl. Opt.*, **41**, 6957–6967.

R. O. Knuteson et al. (2004): Infrared land surface remote sensing using high spectral resolution aircraft observations, *Advances In Space Research*, **33** 1114–1119.

*__J. Li et al. (2007):__ Physical retrieval of surface emissivity spectrum from hyperspectral infrared radiances, *Geophys. Res. Lett.*, **34**, L16812.

#__L. Zhou et al. (2008):__ Regression of surface spectral emissivity from hyperspectral instruments, *IEEE Trans. Geosci. Remote Sensing*, **46**, 328–333.

#__J. Susskind et al. (2008):__ Improved surface parameter retrievals using AIRS/AMSU data, *Proc. SPIE*, **6966**, 10–12.

#__E. Péquignot et al. (2008):__ Infrared Continental Surface Emissivity Spectra Retrieved from AIRS Hyperspectral Sensor, *J. Appl. Meteorol. Climatol.*, **47**, 1619–1633.

*__X. Liu et al. (2009):__ Retrieval of atmospheric profiles and cloud properties from IASI spectra using super-channels, *Atmos. Chem. Phys.*, **9**, 9121–9142.

*__D. K. Zhou at al.__ (2009), All weather IASI single field-of-view retrievals: case study - validation with JAIVEx data, *Atmos. Chem. Phys.*, **9**, 2241–2255.

*__D. K. Zhou at al. (2010):__ Global land surface emissivity retrieved from satellite ultraspectral IR measurements, submitted to *IEEE Trans. Geosci. Remote Sensing*.

Emissivity (ε_ν) is linear to Radiance (R_ν)

$$R_\nu = \varepsilon_\nu B_\nu(T_s)\tau_\nu(p_s \to 0, \theta_{sat}) + \int_{p_s}^{0} B_\nu[T(p)] \frac{d\tau_\nu(p \to 0, \theta_{sat})}{dp} dp$$

$$+ F_\nu^d \rho_\nu^t \tau_\nu(p_s \to 0, \theta_{sat}) + \frac{H_\nu}{\sec(\theta_{sun})} \tau_\nu(0 \to p_s, \theta_{sun}) \rho_\nu^s \tau_\nu(p_s \to 0, \theta_{sat})$$

$$= [\int_{p_s}^{0} B_\nu[T(p)] \frac{d\tau_\nu(p \to 0, \theta_{sat})}{dp} dp + F_\nu^d \tau_\nu(p_s \to 0, \theta_{sat}) + \frac{H_\nu}{\sec(\theta_{sun})\pi} \tau_\nu(0 \to p_s, \theta_{sun}) \tau_\nu(p_s \to 0, \theta_{sat})]$$

$$+ [B_\nu(T_s)\tau_\nu(p_s \to 0, \theta_{sat}) - F_\nu^d \tau_\nu(p_s \to 0, \theta_{sat}) - \frac{H_\nu}{\sec(\theta_{sun})\pi} \tau_\nu(0 \to p_s, \theta_{sun}) \tau_\nu(p_s \to 0, \theta_{sat})] \varepsilon_\nu$$

$$= k_1 + k_2 \varepsilon_\nu$$

The surface is assumed to be Lambertian (or diffuse reflection

$\rho_\nu^t =$ spectral surface reflectivity,$(1-\varepsilon_\nu)$

$\rho_\nu^s =$ spectral solar reflectivity,$(1-\varepsilon_\nu)/\pi$

$R_\nu =$ observed spectral radiance

$\varepsilon_\nu =$ spectral emissivity

$B_\nu =$ spectral Planck function

$T_s =$ surface skin temperature

$\tau_\nu(p_1 \to p_2) =$ spectral transmittance from presp_1 to p_2

$T(p) =$ temperature at pressure$p$

$H =$ solar irradiance

$\theta_{sun} =$ solar zenith angle

$\theta_{sat} =$ sattlite zenith angle

$F_\nu^d =$ down welling thermal flux

Training Dataset & Emissivity Regression

Atmospheric : An all-seasonal-globally representative training database (UW SeeBor Database).

Surface : $T_s = T_a + T_\delta$, where T_δ is a random number generated value with a mean of 0 K and a STD of 3 K over water and 10 K over land. ε is randomly assigned to profile from ε database.

Cloud : Use parameterization of balloon and aircraft cloud microphysical data base to specify cloud effective particle size and cloud optical depth using random number generator to specify visible cloud optical depth within a reasonable range.

$$F(\varepsilon_\nu) = \log[\log(\varepsilon^{HB} - \varepsilon^{LB} + \delta) - \log(\varepsilon^{HB} - \varepsilon_\nu)]$$

- Lab. measured emis. converted to emis. logarithm function $F(\varepsilon)$ to constrain emis. retrieval.

$$A_i^F = \sum_{j=1}^{nch} F_j(\varepsilon)\varphi_{ji}^F$$

- A set of emis. logarithm functions are used to calculate its Eigenvectors and their amplitudes. Emis. amplitudes are used with other other parameters as a state vector to calculate radiance.

$$A_i = \sum_{j=1}^{nc} R_j \varphi_{ji}$$

- A set of radiances are used to calculate its Eigenvectors and their amplitudes.

$$S_j = \sum_{i=1}^{n-1} K_{ji} A_i + K_{jn} P_s = \sum_{i=1}^{n-1} K_{ji} \left(\sum_{l=1}^{nc} R_l \varphi_{li}\right) + K_{jn} P_s$$

- Regression coefficients are generated using a training database (state vector) and their associated radiances. State vector is retrieved with measured radiance. Emis. EOF amplitudes are part of the state vector.

$$\varepsilon_j = \varepsilon^{HB} - \exp[\log(\varepsilon^{HB} - \varepsilon^{LB} + \delta) - \exp(F_j)]$$

$$= \varepsilon^{HB} - \exp[\log(\varepsilon^{HB} - \varepsilon^{LB} + \delta) - \exp(\sum_{i=1}^{9} \varphi_{ji}^F A_i^F)]$$

- Emissivity spectrum is calculated with retrieved emis. EOF amplitudes.

Cloud Detection within Retrieval

Multi-stage regression retrievals are performed. The first-stage involves mixed (i.e., clear and cloudy) regression. The second-stage (e.g., either clear or cloudy) depends on the cloud detection criteria that are based on first-stage retrieved cloud parameters.

Note: ϕ = 0, 1, and 2 are for clear sky, ice cloud, and water clouds, respectively; and H_c is cloud top height relative to surface, ϕ is cloud phase, and τ_{cld} is cloud visible optical depth.

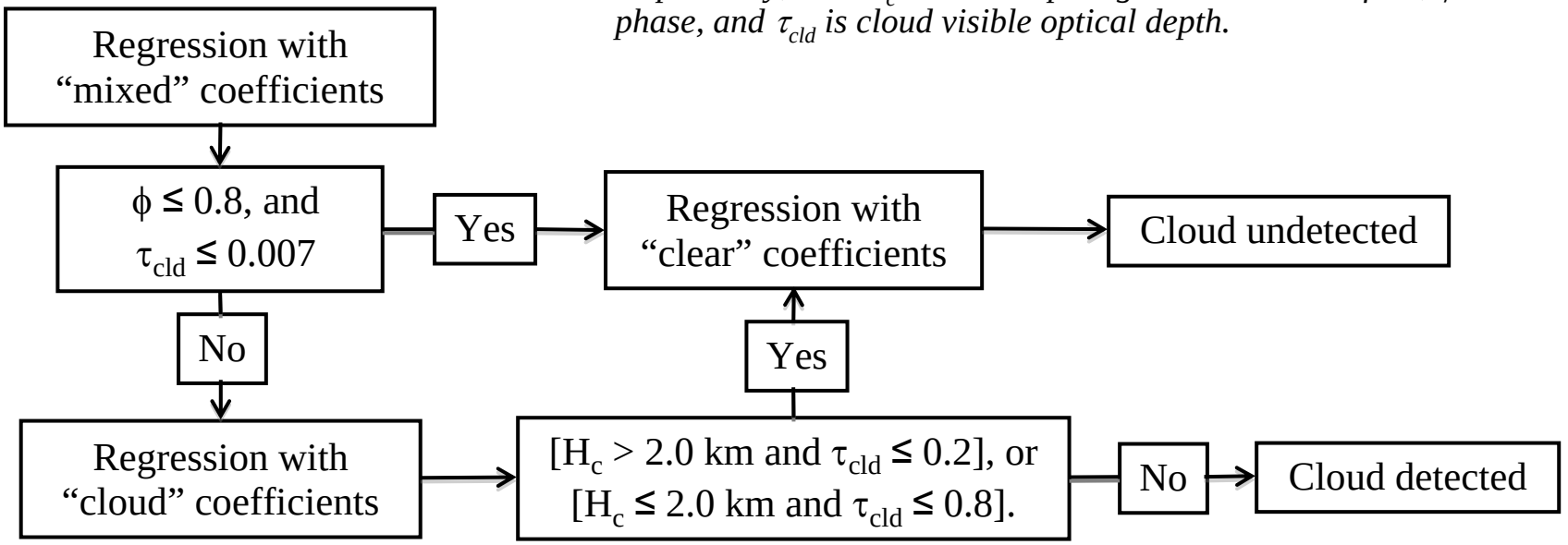

Emis. Accuracy Estimation Under Clear-sky

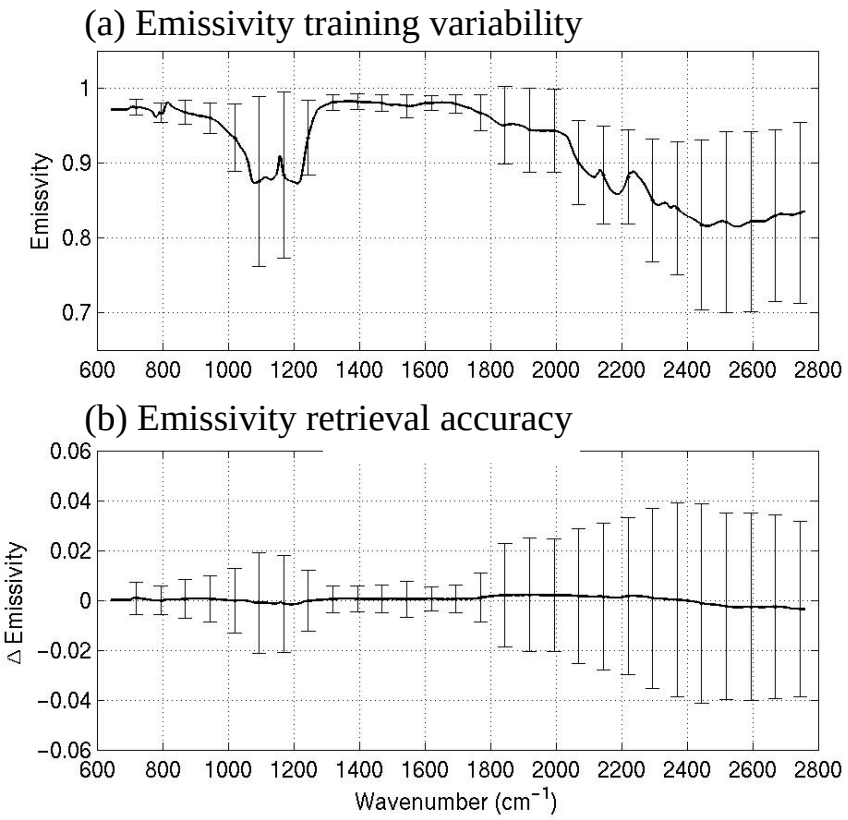

- The emissivity assigned to each training profile is randomly selected from a laboratory measured emissivity database, indicated in panel **a**, and has a wide variety of surface types suitable for different geographical locations. The vertical bars show the emissivity STD for this dataset.
- Estimated surface emissivity retrieval accuracy, the mean difference (or bias) in curve and the STDE in vertical bars shown in panel **b**, is training data dependent.

Note: since the emissivity is linear to channel radiances, we chose to use retrieved emissivity from linear EOF regression, not further retrieved in physical iteration. However, if the physical retrieval is performed for other parameters, emissivity will be further refined through physical iteration.

Emis. Ret. and Rad. Fitting Samples

Over Sahara (Lat.=23.38° N; Lon.=24.41° E);
Daytime (SZA=30.5°), 2007.08.01

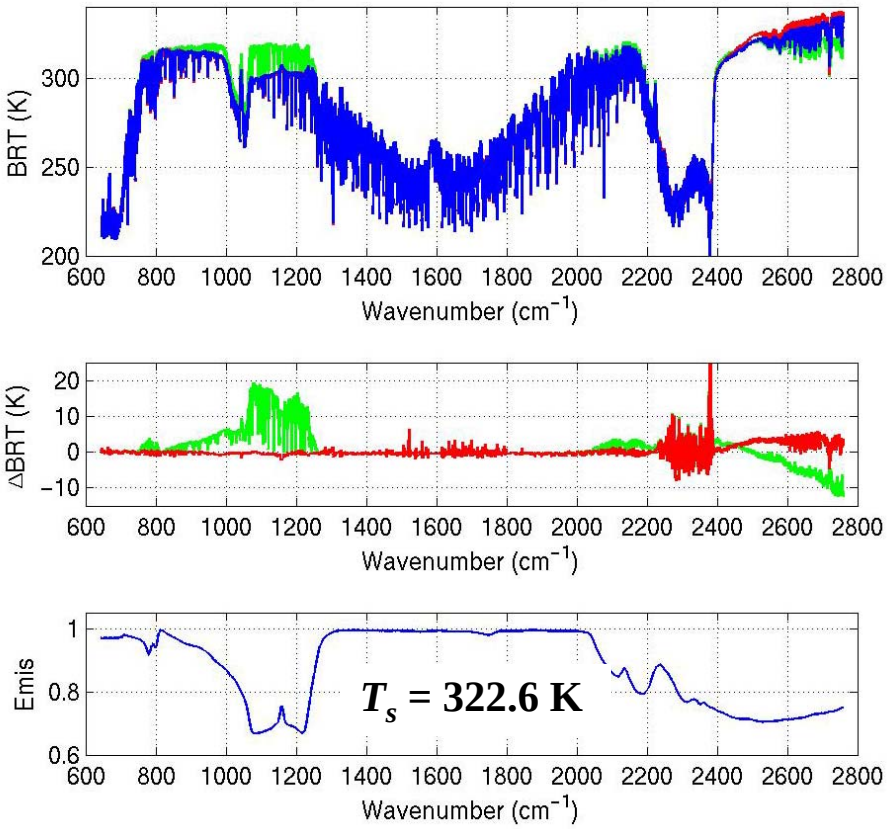

Over Sahara (Lat.=23.41° N; Lon.=24.83° E);
Nighttime (SZA=120.6°), 2007.08.01

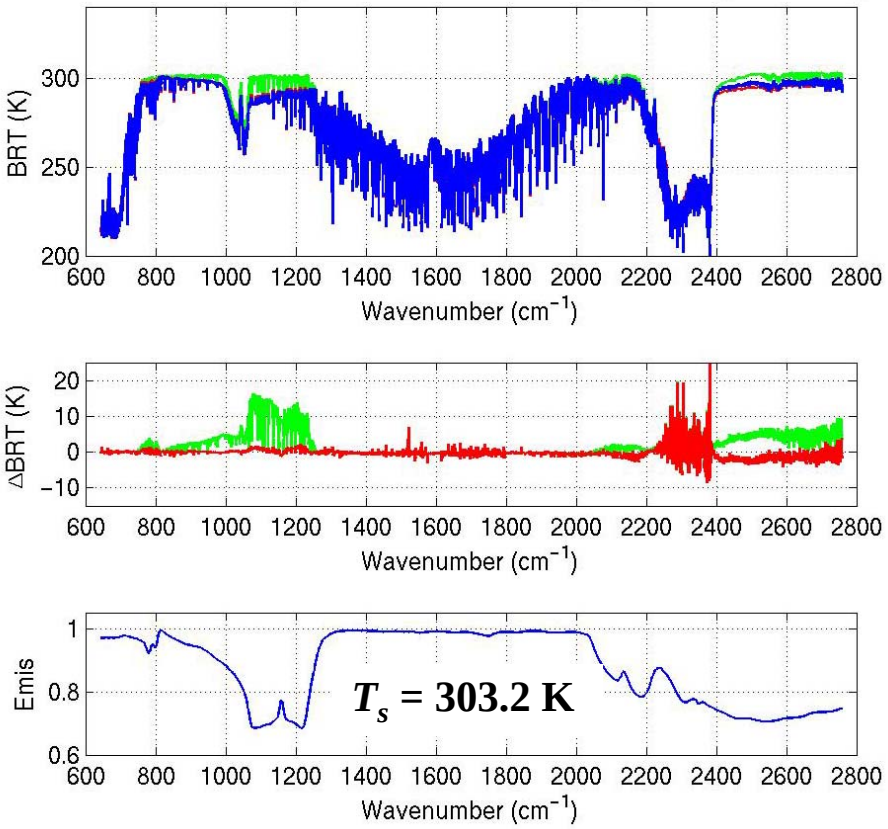

It is to demonstrate that the technique separates surface emissivity from skin temperature:

Samples shown are for both day and night observations over the Sahara Desert. Simulated spectral radiances (with rtv emis in red curves; emis of 1 in green curves) are plotted in comparison with the measurements (blue curves). Retrieved surface emissivity spectra are plotted in the bottom panels with IASI day and night observations, respectively.

Namib and Kalahari Deserts for ε Evaluation

G. C. Hulley, S. J. Hook, E. Manning, S.-Y. Lee, and E. Fetzer, "Validation of the Atmospheric Infrared Sounder (AIRS) version 5 land surface emissivity product over Namib and Kalahari deserts," *J. Geophys. Res.*, vol. 114, no. D1, pp. 9104.1–9104.11, Oct. 2009.

- **Kalahari:** The majority of the sand lies on the level plains of the Kalahari Basin, sand dunes mixed with grassy scrublands and sparse trees.

- **Namib:** The vast expanse of shifting dunes is almost completely devoid of vegetation except for sparse perennial grasses.

- Different sand mineralogy from Namib to Kalahari sites.

Table 1. Summary of the Major Characteristics of the Kalahari and Namib Validation Sites Including Locality, Elevation, Surface Area, Dune Height, Grain Size, Sand Source and Bulk Mineralogy

	Kalahari	Namib
Locality	covers most of Botswana, including northwestern South Africa and southeastern Namibia	western coast of Namibia
Approximate surface area (km^2)	100,000	34,000
Elevation (m)	1,000	0–500
Maximum dune height (m)	30	300
Percent of grain size of sand		
>500 μm	0%	1%
250–500 μm	30%	53%
125–250 μm	68%	40%
<125 μm	2%	6%
Sand source	aeolian deposited, fluvial	littoral, fluvial, weathered tsondab sandstone
Mineralogy		
Major	Quartz	quartz
Minor		feldspar, magnetite

Temporal Variation over Namib and Kalahari

Namib: Lat.=24.75±0.15° S;

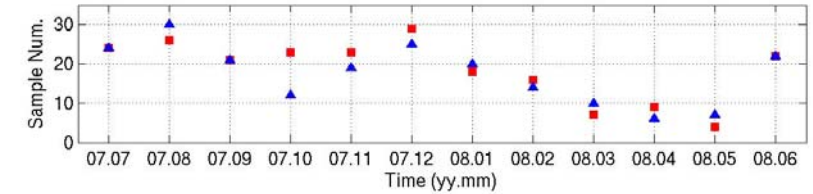

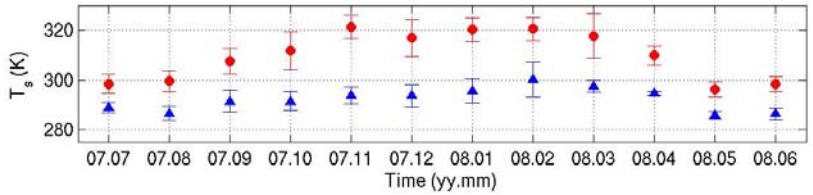

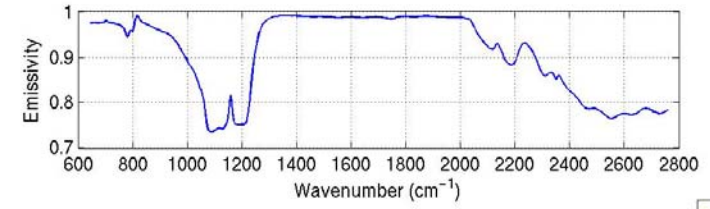

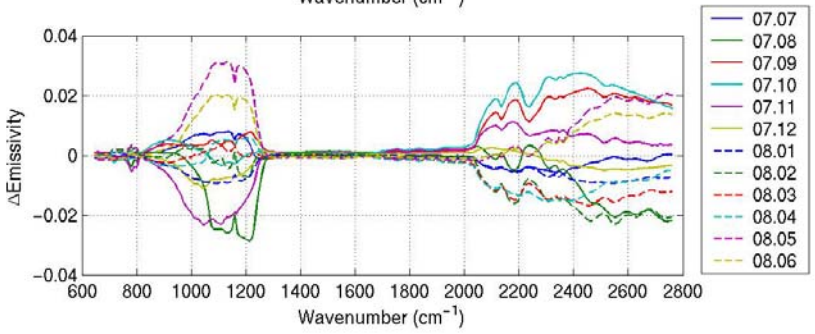

Kalahari: Lat.=24.75±0.15° S;

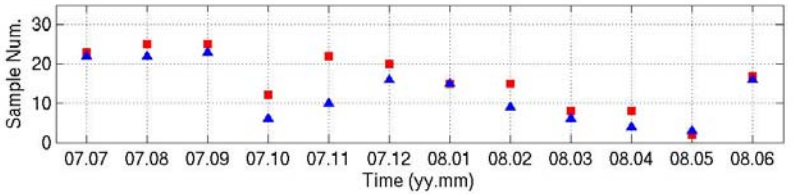

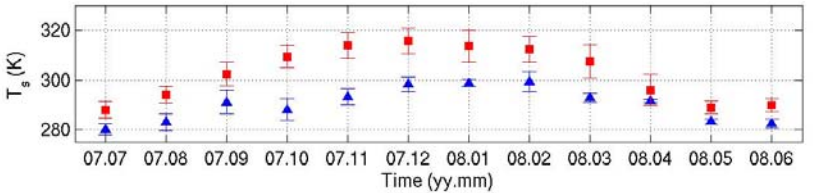

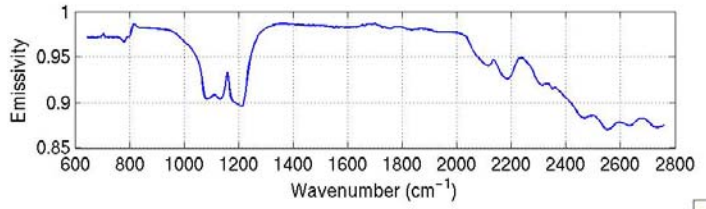

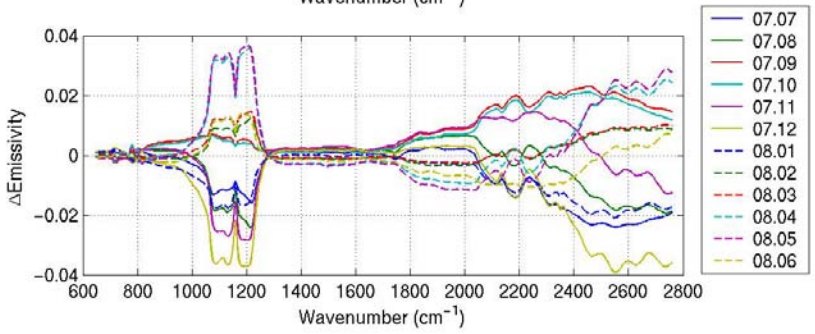

Emis. temporal variation is $\zeta_\nu = \left(\frac{\varepsilon_\nu^{\max} - \varepsilon_\nu^{\min}}{1 - \bar{\varepsilon}_\nu} \right) 100\%$. ζ_{1150} (Namib) = 23.2%; ζ_{1150} (Kalahari) = 71.4%

Emissivity Validation / Evaluation

- We will use the Namib site for absolute validation and the Kalahari site for relative spectral-shape validation.

- The quartz-doublet region from the Namib to the Kalahari site, is well captured by retrievals, due to the different sand mineralogy at these 2 sites.

Kalahari Site

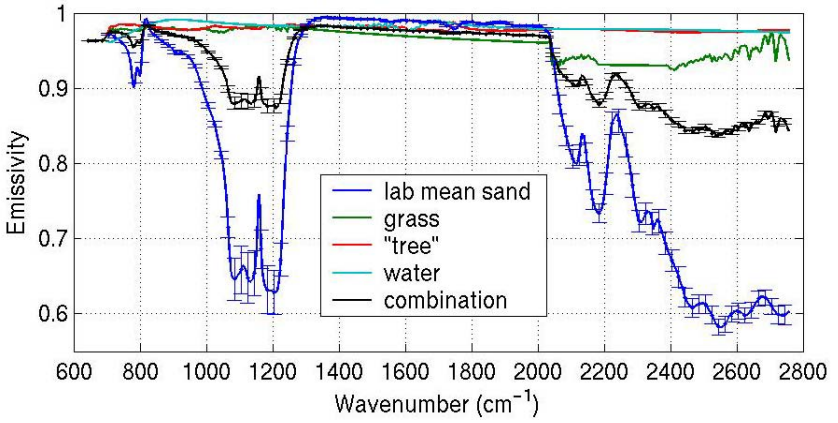

Namib Site

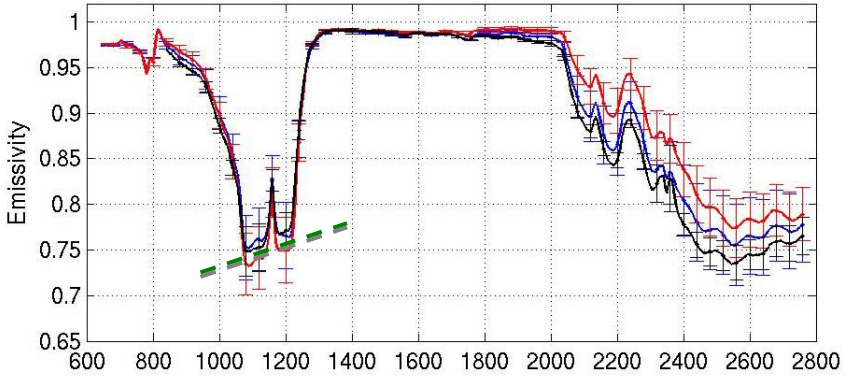

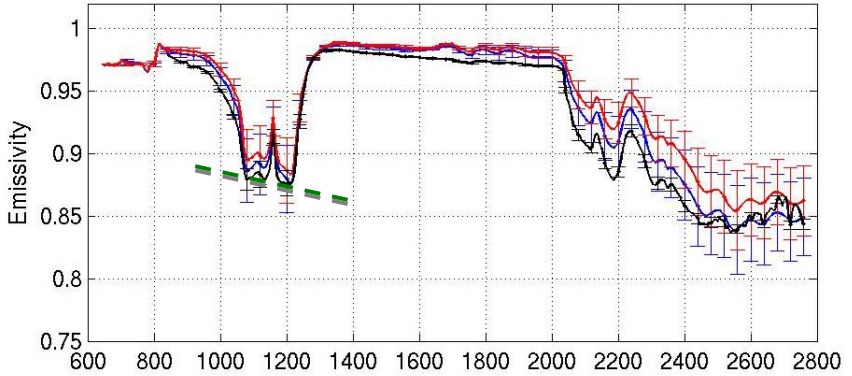

Quality Filter for Global Assembled Mean

Cloud filtering and outlier rejection:

- Due to cloud coverage, not every measurement can provide surface parameters; however, the surface parameters can be retrieved under optically thin clouds with a relatively poor accuracy in comparison with that retrieved under clear-sky conditions.
- The surface emissivity composition can be assembled over a period of time and area. Single retrievals within a spatial grid (area) meeting the Quality Filter criteria will be taken to generate a mean emissivity.

Q.F. criteria are listed as:

1. $\tau_{cld} \le 0.5$,
2. $\left| A_1^F - \overline{A_1^F} \right| \le std(A_1^F)$, and
3. $\left| A_2^F - \overline{A_2^F} \right| \le std(A_2^F)$.

April 2009 – Rub' al Khali, Saudi Arabia [21.25° < lat. ≤ 21.75° ; 54.25° < lon. ≤ 54.75°]

All Retrievals (149 rtv.) | Pass filter 1 (137 rtv.) | Pass filter 1-2 (92 rtv.) | Pass filter 1-3 (65 rtv.)

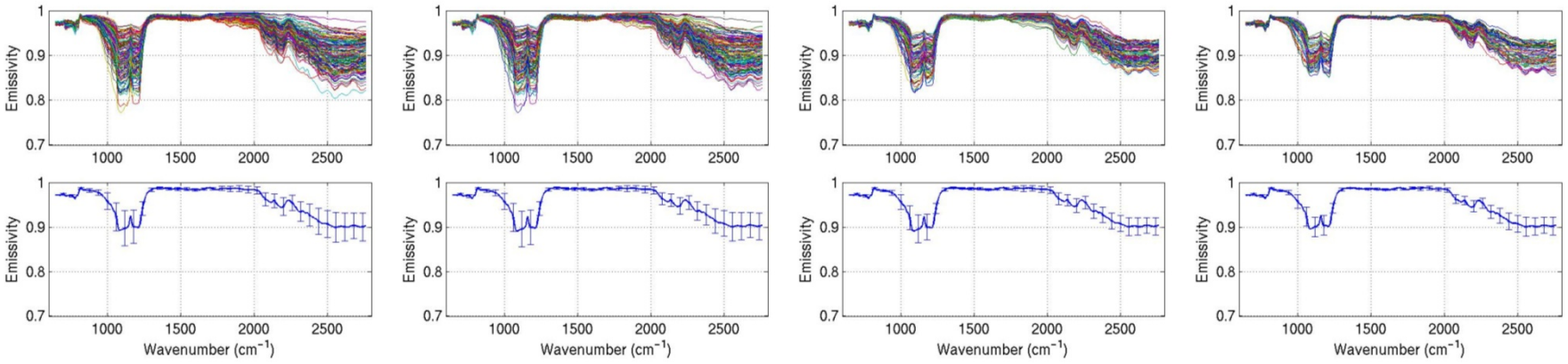

Monthly-Mean Land T_s and ε_{1140} (0.5-deg scale)

(a) July 2007: T_s (K)

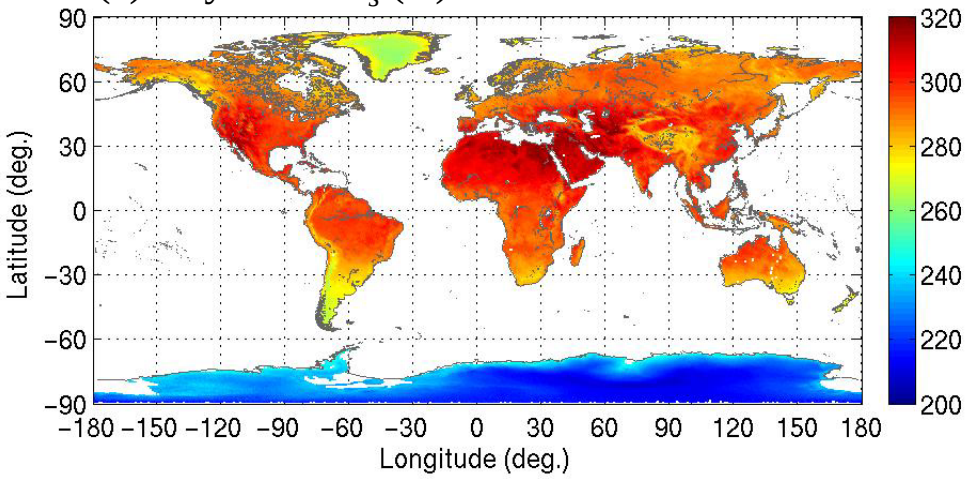

(b) July 2007: ε at 1140 cm^{-1}

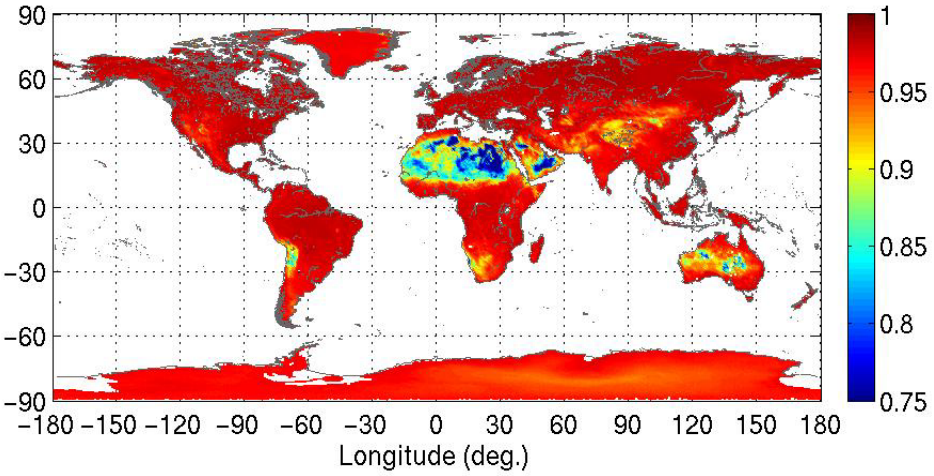

(c) January 2008: T_s (K)

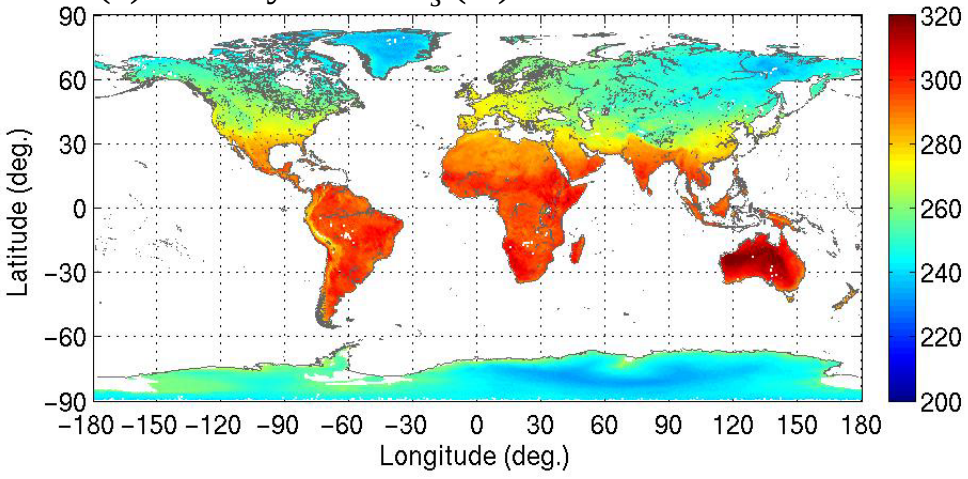

(d) January 2008: ε at 1140 cm^{-1}

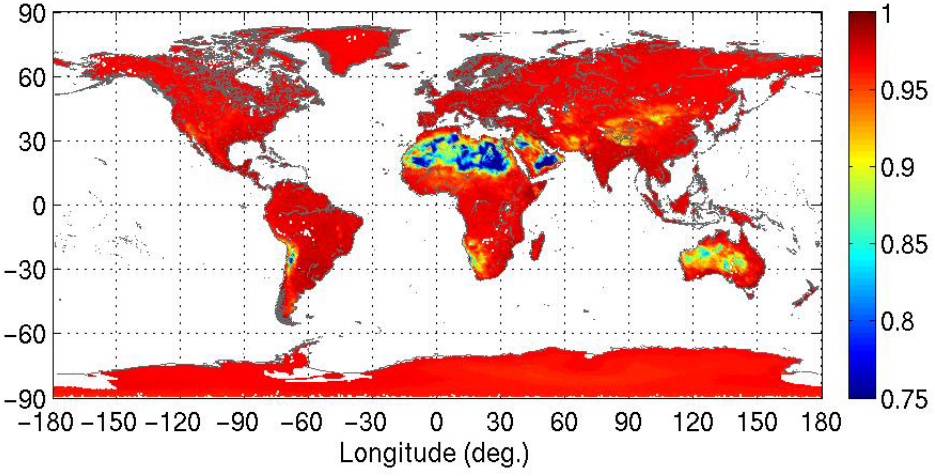

Langley Research Center

ε_{950} Seasonal Variation

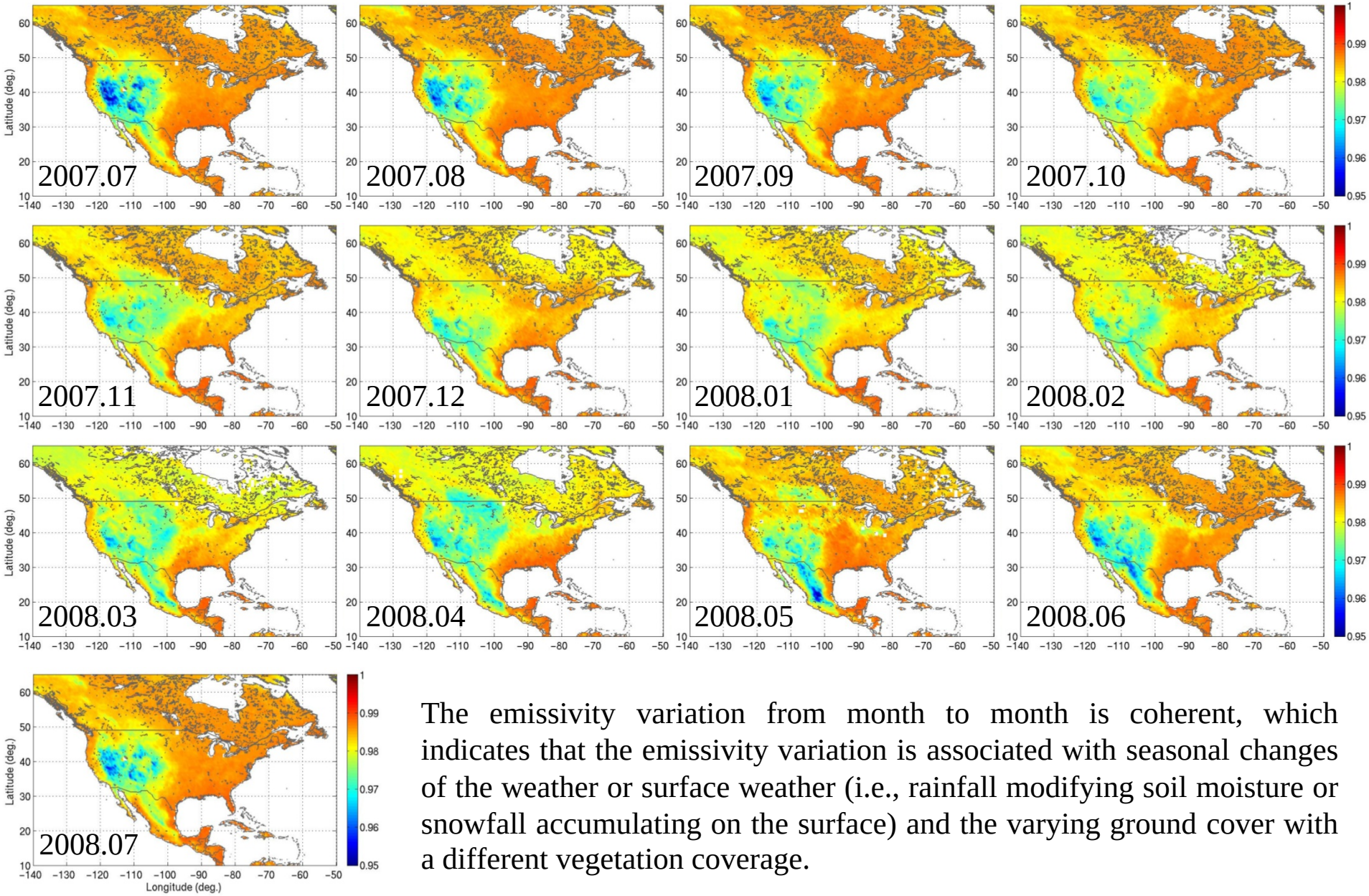

The emissivity variation from month to month is coherent, which indicates that the emissivity variation is associated with seasonal changes of the weather or surface weather (i.e., rainfall modifying soil moisture or snowfall accumulating on the surface) and the varying ground cover with a different vegetation coverage.

Langley Research Center

ε_{950} Seasonal Variation

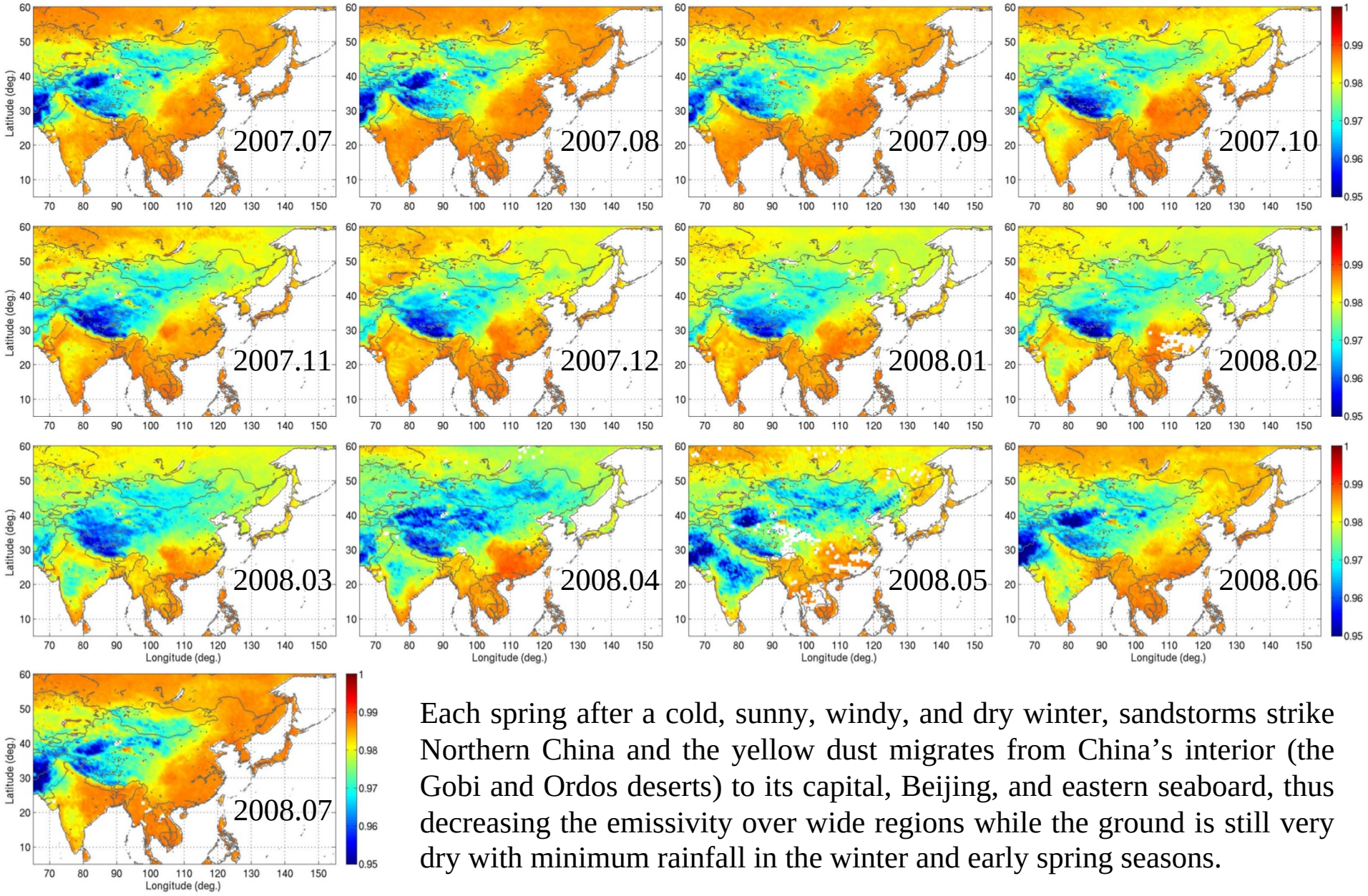

Each spring after a cold, sunny, windy, and dry winter, sandstorms strike Northern China and the yellow dust migrates from China's interior (the Gobi and Ordos deserts) to its capital, Beijing, and eastern seaboard, thus decreasing the emissivity over wide regions while the ground is still very dry with minimum rainfall in the winter and early spring seasons.

Summary and Future Work

- A state-of-the-art retrieval algorithm, dealing with all-weather conditions, has been developed and applied to IASI radiance measurements. Surface emissivity is retrieved using multi-stage linear EOF physical-regressions.
- Initial emissivity validation over the Namib and Kalahari deserts is performed. IASI Emissivity retrieval accuracy under clear-sky conditions is estimated that a STDE is about 0.02 and 0.04 for longwave and shortwave window regions, respectively.
- Results from IASI retrievals indicate that surface emissivity retrieved with satellite IR ultraspectral data can capture different land surface type properties. The seasonal variation of global land surface emissivity derived from satellite IR ultraspectral data is evident.
- Operational satellite IR ultraspectral data can provide information for monitoring the Earth's environment and global change as well as the study of ecosystem health that plays an important role in understanding the impact of climate change and human activity on altered degradation, biodiversity, and ecosystem sustainability.
- Focus on emissivity validation/evaluation for providing more-definitive accuracy of the emissivity products. Algorithm improvements, along with its product validation, will be made and applied to current and future satellite instruments to provide data for long-term monitoring of the Earth's environment and for climate studies.
- Produce IASI/AIRS emissivity and surface skin temperature (from May 2002) to current and future operational IASI and CrIS for monitoring global change.

International TOVS Study Conference, 17th, ITSC-17, Monterey, CA, 14-20 April 2010. Madison, WI, University of Wisconsin-Madison, Space Science and Engineering Center, Cooperative Institute for Meteorological Satellite Studies, 2011.